Refluxing synthesis of Mn-doped ZnO nanoparticles and their applications in dielectric ceramics

Ye Zhao, Fan Tong, Rong Yang, Xiao Qu, Mao-Hua Wang ✉

School of Petrochemical Engineering, Changzhou University, Changzhou 213164, People's Republic of China
✉ *E-mail: 627907188@qq.com*

Published in Micro & Nano Letters; Received on 19th March 2018; Revised on 20th July 2018; Accepted on 12th October 2018

Pure and manganese (Mn)-doped zinc oxide (ZnO) (0, 1, 2 and 4 wt%) nanoparticles are synthesised by refluxing method. The as-synthesised nanoparticles are characterised by X-ray powder diffraction, Fourier transform infrared spectroscopy, transmission electron microscopy and energy-dispersive X-ray spectroscopy (EDS). The results show that pure and Mn-doped ZnO nanoparticles have a hexagonal wurtzite structure and the (101) diffraction peaks position of Mn-doped ZnO shift toward the smaller value of diffraction angle compared with pure ZnO powders, confirming that the Mn^{2+} were well incorporated into ZnO crystal lattice. Moreover, Mn doping also restrained the growth of particles and the size decreased from 14.9244 to 13.1196 nm with the increase in doping concentration from 0 to 4 wt%. The EDS analysis for 2 wt% Mn-doped ZnO confirms the presence of Mn in ZnO nanocrystal. The dielectric measurements show that Mn-doped ZnO ceramics exhibit higher dielectric constant, while dielectric constant and dielectric loss increased continuously with the temperature increased. In addition, 2 wt% Mn-doped ZnO ceramics showed the high dielectric constant (23×10^3) and low dielectric loss (0.95) at 125°C after sintering at 1000°C for 2 h.

1. Introduction: Semiconductor nanomaterials have generated great interest in the past years due to quantum size effects and their unique properties and among these semiconductor nanomaterials, zinc oxide (ZnO) is gaining more interest because it is abundant, inexpensive and non-toxic. ZnO is an n-type semiconductor oxide with wurtzite structure, a wide direct bandgap of 3.37 eV at room temperature and a large exciton binding energy of about 60 meV [1]. Therefore, ZnO nanoparticles are used in the fabrication of solar cells [2], gas sensors [3, 4], luminescent materials [5], varistors [6], field-emission transistors [7], photocatalysis [8] and DNA sequence detectors [9]. In summary, among all the semiconducting nanomaterial ZnO has attracted the scientific community as a multifunctional semiconducting material [10–13].

The dielectric properties of materials that are of interest in most applications can be defined in terms of their relative permittivity. Permittivity is a complex quantity generally used to describe the dielectric properties that influence reflection of electromagnetic waves at interfaces and the attenuation of the wave energy within materials [14]. Material with high dielectric constant and low loss are always very essential to be used in microwave telecommunications, multilayer capacitor, dynamic random access memory and microwave integrated circuits [15, 16]. In recent years, ZnO nanomaterials have been studied as conductive fillers in polymers with high dielectric constant and they have received much more attention for their promising application in high charge-storage capacitors [17, 18]. It is well known that the various properties of semiconductor materials can be enhanced and/or modified by doping. The dielectric properties can be improved by doping the conductive material with an impurity element [19]. The effects of the dielectric properties of transition and non-transition metal elements (nickel, chromium, lithium)-doped ZnO have been investigated, but the results for dielectric behaviour of ZnO have not been conclusively given out [20–22]. Furthermore, we have found that manganese (Mn)-doped ZnO nanostructures have been studied. The incorporation of Mn into ZnO nanostructures improved optical properties [23], AC-electrical response [24] as well as magnetic properties [25]; however, dielectric properties of Mn-doped ZnO nanoparticles were not studied. ZnO nanostructures with different morphologies and dopants were obtained using different techniques such as precipitation, sol–gel, hydrothermal and reflux method [26–30]. The last direct reflux method has attracted a lot of attention due to its simplicity and cost-effectiveness. In this work, well-dispersed Mn-doped ZnO nanoparticles with small crystal sizes were prepared by reflux method and their dielectric properties were studied as a function of temperature.

2. Experimental results

2.1. Materials used: Zinc acetate dihydrate ($ZnAc_2{\cdot}2H_2O$) and manganous chloride ($MnCl_2$) were purchased from Sinopharm Chemical Reagent Co., Ltd. Ethylene glycol was supplied by Shanghai Lingfeng Chemical Reagent Co., Ltd. All reagents used were analytic grade and used without further purification.

2.2. Synthesis: In the typical experiment, 8.78 g $ZnAc_2{\cdot}2H_2O$ and corresponding amounts of $MnCl_2$ (0, 1, 2 and 4 wt%) were added into 150 ml of ethylene glycol and stirred until the solution became homogeneous. Then, the mixed solution was heated at 170°C under reflux for 2 h. The precipitate was washed with absolute ethanol and deionised water and dried at 80°C.

2.3. Preparation of the ZnO discs for dielectric measurements: These obtained powders were granulated and uniaxially pressed into discs with a 1.2 mm thickness and an 11 mm diameter. The discs were sintered at 1000°C for 2 h in static air. The silver paste was used to coat both sides of the sintered discs, followed by firing at 55°C for 15 min to form electrodes in order to measure dielectric properties.

2.4. Characterisation: Samples were characterised by X-ray powder diffraction (XRD; Rigaku D/MAX-YA) using copper Kα radiation ($\lambda = 0.154$ nm) at the scanning rate of 5°/min in a 2θ range from 10° to 80°. The morphology and structure of the samples were characterised by transmission electron microscopy (TEM, JEM-2100, Japan) operated at 200 kV. Dielectric properties were measured using a Heinrich Lenz Capacitance Resistance (LCR) meter (AT821, China) controlled by a computer at 1 kHz.

3. Result and discussion

3.1. X-ray analysis: Fig. 1*a* shows XRD patterns of pure and doped ZnO nanoparticles. All the diffraction peaks corresponding could

doi: 10.1049/mnl.2018.5397

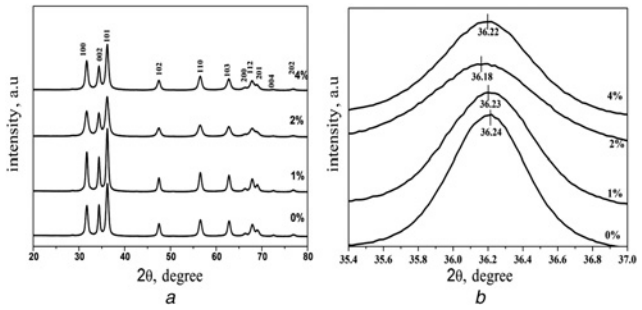

Fig. 1 *X-ray diffraction patterns of Mn-doped ZnO powder*
a X-ray diffraction patterns of Mn-doped ZnO powder
b The expanded X-ray diffractogram of (101) peak

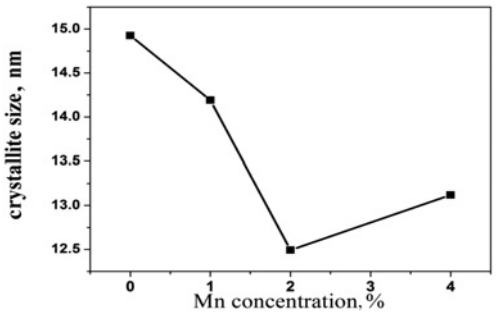

Fig. 2 *Variation of crystallite size for Mn-doped ZnO samples*

be attributed to the wurtzite structure (JCPD-36–1451) and no other phases were found, suggesting that the Mn element may be doped into ZnO [31]. Fig. 1*b* shows the magnified region of (101) peak, clearly indicates a shift to lower 2θ values with increasing concentration of Mn. This shifting was due to the difference in ionic radii of Mn^{2+} (0.60 nm) and Zn^{2+} (0.66 nm) observed in similar samples. Thus, the peak shift in various Mn-doped ZnO provides conclusive evidence for the substitution of Mn^{2+} into the ZnO lattice [32, 33]. In addition, the width of diffraction peaks increases with an increase of Mn doping level, which means that the crystallite size decreases with the increase of Mn content [34].

The lattice parameters (a and c) of prepared samples were obtained from the equation below:

$$\frac{1}{d^2} = \frac{4}{3}\left(\frac{h^2 + hk + k^2}{a^2}\right) + \frac{l^2}{c^2} \tag{1}$$

where h, k and l are Miller's indices. The volume of the hexagonal closely packed unit cell was calculated using the formula below:

$$V = \frac{\sqrt{3}}{2}a^2c = 0.866a^2c \tag{2}$$

The crystallite size for all the samples was calculated using Scherrer's formula below:

$$D = \frac{0.9\lambda}{\beta\cos\theta} \tag{3}$$

where λ is the wavelength of X-ray radiation, β is the full width at half maximum of the peaks at the diffracting angle θ [35]. The crystal size, lattice parameters and volume of all samples are shown in Table 1. The data shows that the presence of Mn^{2+} in ZnO prevented the growth of crystal grains. Fig. 2 shows the variation of crystallite size with the content of Mn doped into ZnO nanostructure.

Table 1 Variation of crystallite size, lattice parameters and unit cell volume with a doping concentration

Mn concentration, %	Crystallite size, nm	Lattice parameter		Unit cell volume, Å^3
		a, Å	c, Å	
0	14.9244	3.2530	5.2098	47.8073
1	14.1904	3.2552	5.2098	47.8830
2	12.4920	3.2564	5.2156	47.8958
4	13.1196	3.2569	5.2126	47.7427

3.2. Fourier transform infrared spectroscopy (FTIR) analysis: Fig. 3 shows FTIR patterns of all the samples. The broad absorption peak appeared at 3420 cm^{-1} indicating O–H stretching vibrations. The strong absorption band at 1624 cm^{-1} was assigned to the Brownsted acidity (C = O band). The peaks at 1445 cm^{-1} show the presence of Lewis acidity (C = C bond) in the molecule and the relatively broad bands at around 869 cm^{-1} are assigned to the vibrational frequencies due to the change in the microstructure due to the Mn incorporation into ZnO lattice. The stretching of the ZnO bond corresponds to the frequency at 445 cm^{-1}1 for pure ZnO. This peak shifts to higher frequencies: 452 cm^{-1} for 1 wt% Mn, 454 cm^{-1} for 2 wt% Mn and 465 cm^{-1} for 4 wt% Mn. It is worth noting that these results confirm a well-established theory of vibrational modes in mixed and doped crystals, mainly, that ion substitution should result in a downward shift of the transverse optical phonon mode.

3.3. TEM, field-emission SEM (FE-SEM) and energy-dispersive X-ray spectroscopy (EDS) analysis: To further characterise the morphological properties of Mn-doped ZnO nanoparticles and their ceramics, Figs. 4*a* and *b* displayed the TEM images of the 0 and 2 wt% Mn-doped ZnO powders by refluxing method. Fig. 4*a* shows pure ZnO nanocrystals (15–25 nm) that are spatially connected to form a porous and spherical cluster. In addition, the sizes of particles are not uniform. Fig. 4*b* shows more uniform and well-dispersed spherical Mn-doped ZnO nanoparticles with a particle size of about 10–20 nm. The composition of 2 wt% Mn-doped ZnO nanoparticles is detected by EDS in Fig. 5. From spectra, it can be seen that Zn and O appeared as the main components with low levels of Mn which confirms the successful doping of Mn in the ZnO host structure and substantiates the results obtained by XRD analysis. The molar content of each element is

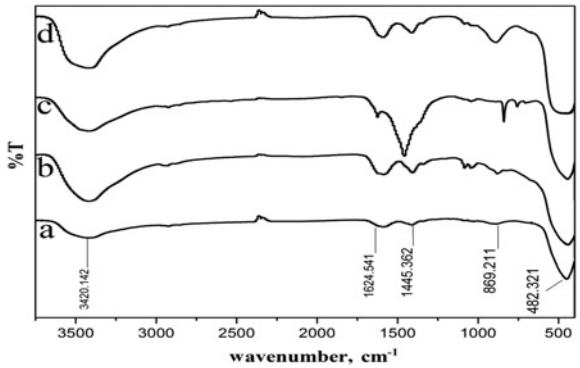

Fig. 3 *FTIR spectra of ZnO doped with different contents of Mn*
a 0%
b 1%
c 2%
d 4%

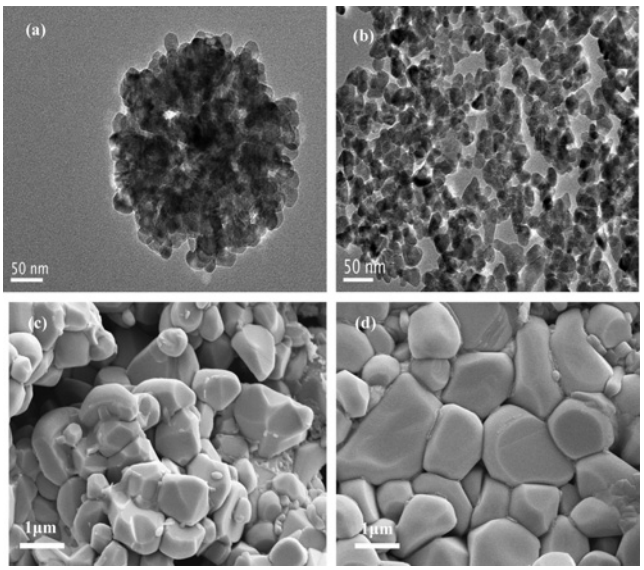

Fig. 4 *TEM images of*
a 0wt% Mn-doped ZnO nanoparticles
b 2 wt% Mn-doped ZnO nanoparticles
FE-SEM images of
c 0 wt% Mn-doped ZnO ceramics
d 2 wt% Mn-doped ZnO ceramics

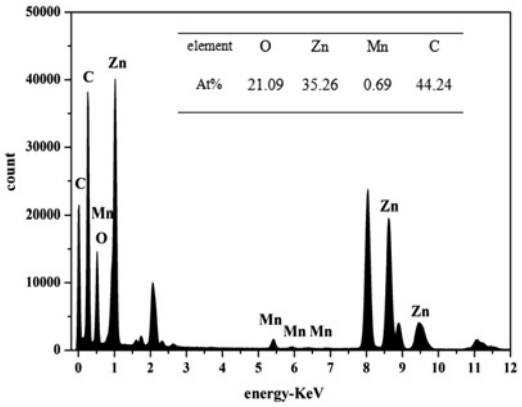

Fig. 5 *EDS spectrum ZnO nanoparticles doped with 2% Mn*

shown in the table. The values of the atomic percentages of Mn/metal ion ratio was very close to their nominal stoichiometry and were within the experimental error. FE-SEM image of pure and 2 wt% Mn-doped ZnO ceramics was shown in Figs. 4*c* and *d*. As shown in Fig. 4*c*, the grain size in pure ZnO ceramic was about 0.5–1.2 μm, the grain boundary was not clear and shows more pores. On further increase of doping amount from 0 to 2 wt%, the grain size was about 0.8–2 μm. A dense microstructure with obvious grain and grain boundary structures are observed in Fig. 4*d*. Such microstructures are extremely useful in improving the dielectric properties of ZnO ceramics [36].

3.4. Dielectric constant: The dielectric constant (ε) was determined from the following equation [37]:

$$\frac{14.4Cd}{D^2} \tag{4}$$

where C is the capacitance, d and D are the thickness and diameter of the ceramic disc. Dielectric loss (tan δ) represents a dissipated energy in a dielectric system.

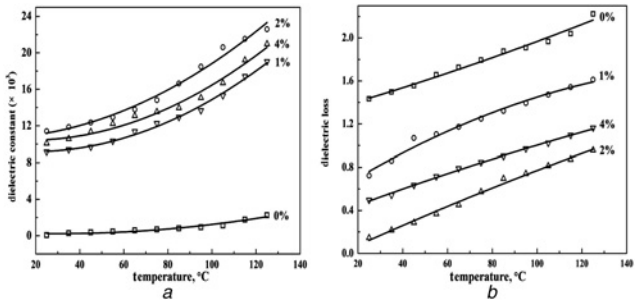

Fig. 6 *Temperature dependences of*
a Dielectric constant for different samples after sintering at 1000°C:
b Tan δ for different samples after sintering at 1000°C

Fig. 6 presents the temperature dependence of the dielectric constant and dielectric loss for different samples at a frequency of 1 kHz. From Fig. 6*a*, it can be seen that the value of the dielectric constant of pure ZnO was relatively lower than for Mn-doped ZnO. The dielectric constant of doped samples continuously increased with temperature from 20 to 125°C even though the rates of these enhancements were not the same. It can be obviously seen that 2 wt% Mn-doped ZnO ceramic exhibited the highest dielectric constant.

Dielectric loss (tan δ) also increased with increasing temperature in Fig. 6*b*. Doped ZnO showed lower dielectric loss compared with pure ZnO. Nanoparticles doped with 2 wt% Mn showed the lowest dielectric loss. Thus, ZnO ceramic doped with 2 wt% Mn sintered at 1000°C shows the highest dielectric constant (11.1942×10^3–22.395×10^3) and lowest dielectric loss (0.145–0.9568) in the temperature range from 20 to 125°C.

4. Conclusions: In this Letter, we have successfully synthesised Mn-doped ZnO nanoparticles with 0, 1, 2 and 4 wt% Mn by using a reflux method. All the prepared nanoparticles exhibited hexagonal ZnO lattice structure and the width of diffraction peaks increases with an increase of Mn doping level, whereas crystal size decreased with the increase of dopant concentration. TEM images of Mn-doped ZnO with different contents show that the particles consisted of a large amount of well-dispersed nanospheres. The dielectric properties of Mn-doped ZnO ceramics are superior to that of pure ZnO. The 2 wt% Mn-doped ZnO ceramic showed the highest dielectric constant (23×103) and lowest dielectric loss (0.95) at 125°C after sintering at 1000°C for 2 h. These properties are very valuable for the fabrication of ceramic capacitor equipment in the near future.

5. Acknowledgment: This work was financially supported by the Changzhou Science, Technology Innovation Project, Production-teaching-research project of Changzhou University Institute of Huaide.

6 References

[1] Viswanatha R., Santra P.K., Dasgupta C., *ET AL.*: 'Growth mechanism of nanocrystals in solution: ZnO, a case study', *Phys. Rev. Lett.*, 2007, **98**, (25), pp. 255501–255504
[2] Matsubara K., Fons P., Iwata K., *ET AL.*: 'ZnO transparent conducting films deposited by pulsed laser deposition for solar cell applications', *Thin Solid Films.*, 2003, **s431–432**, (431), pp. 369–372
[3] Zhang Q., Xie C., Zhang S., *ET AL.*: 'Identification and pattern recognition analysis of Chinese liquors by doped nano ZnO gas sensor array', *Sens. Actuators B, Chem.*, 2005, **110**, (2), pp. 370–376
[4] Lin H.M., Tzeng S.J, Hsiau P.J., *ET AL.*: 'Electrode effects on gas sensing properties of nanocrystalline zinc oxide', *Nanostruct. Mater.*, 1998, **10**, (3), pp. 465–477
[5] Zhou Z.F., Qin F.W., Zang H.R., *ET AL.*: 'Influence of N_2 flux on InN film deposition on sapphire (0001) substrates by ECR-PEMOCVD', *Chin. Phys. Lett.*, 2011, **28**, (2), p. 028102

doi: 10.1049/mnl.2018.5397

[6] Pillai S., Kelly J., Ramesh R., *ET AL.*: 'Advances in the synthesis of ZnO nanomaterials for varistor devices', *J. Mater. Chem. C*, 2013, **1**, (20), pp. 3268–3281

[7] Arnold M.S., Avouris P., Pan Z.W., *ET AL.*: 'Field-effect transistors based on single semiconducting oxide nanobelts', *J. Phys. Chem. B*, 2003, **107**, (3), pp. 659–663

[8] Awad M.A., Ibrahim E.M.M., Ahmed A.M.: 'One step syntheses of S incorporated ZnO nanowires for photocatalysis applications', *Eur. Phys. J. Appl. Phys.*, 2015, **72**, (3), p. 30303

[9] Kumar N., Dorfman A., Hahm J.: 'Ultrasensitive DNA sequence detection using nanoscale ZnO sensor arrays', *Nanotechnology*, 2006, **17**, (12), pp. 2875–2881

[10] Dutta S., Chattopadhyay S., Sarkar A., *ET AL.*: 'Role of defects in tailoring structural, electrical and optical properties of ZnO', *Prog. Mater. Sci.*, 2009, **54**, pp. 89–136

[11] Heoa Y.W., Nortona D.P., Tiena L.C., *ET AL.*: 'ZnO nanowire growth and devices', *Mater. Sci. Eng. R*, 2004, **47**, pp. 1–47

[12] Wang Z.L.: 'ZnO nanowire and nanobelt platform for nanotechnology', *Mater. Sci. Eng. R*, 2009, **64**, pp. 33–71

[13] Özgür Ü., Alivov Y.I., Liu C., *ET AL.*: 'A comprehensive review of ZnO materials and devices', *J. Appl. Phys.*, 2005, **98**, (4), p. 041301

[14] Sosa Morale S.M.E., Valerio-Junco L., López-Malo A., *ET AL.*: 'Dielectric properties of foods: reported data in the 21st century and their potential applications', *LWT-Food Sci. Technol.*, 2010, **43**, pp. 1169–1179

[15] Shaw T.M., Troliermckinstry S., Mcintyre P.C.: 'The properties of ferroelectric films at small dimensions', *Annu. Rev. Mater. Res.*, 2000, **30**, (1), pp. 263–298

[16] Tripathi R., Kumar A., Bhart C., *ET AL.*: 'Dielectric relaxation of ZnO nanostructure synthesized by soft chemical method', *Curr. Appl. Phys.*, 2010, **10**, (2), pp. 676–681

[17] Fernández-Hevia D., Peiteado M., Frutos J.D., et al: 'Wide range dielectric spectroscopy of ZnO-based varistors as a function of sintering time', *J. Eur. Ceram. Soc.*, 2004, **24**, (6), pp. 1205–1208

[18] Samuel M.S., Koshy J., Chandran A., *ET AL.*: 'Electrical charge transport and dielectric response in ZnO nanotubes', *Curr. Appl. Phys.*, 2011, **11**, (4), pp. 1094–1099

[19] Quan B., Liang X., Ji G., *ET AL.*: 'Dielectric polarization in electromagnetic wave absorption: review and perspective', *J. Alloys Compd.*, 2017, **728**, pp. 1065–1075

[20] Yadav H.K., Sreenivas K., Gupta V., *ET AL.*: 'Raman spectroscopy and dielectric studies of multiple phase transitions in ZnO:Ni', *Appl. Phys. Lett.*, 2008, **92**, (12), p. 3753

[21] An N., Lee H., Sharma S.K., *ET AL.*: 'Ferroelectric polarization-induced memristive hysteresis behaviors in Ti- and Mn-codoped ZnO', *J. Korean Phys. Soc.*, 2016, **68**, (7), pp. 869–874

[22] Sharma S., Vyas R., Sharma N., *ET AL.*: 'Highly efficient green light harvesting from Mg doped ZnO nanoparticles: structural and optical studies', *J. Alloys Compd.*, 2013, **552**, (552), pp. 208–212

[23] Othman A.A., Osman M.A., Ibrahim E.M.M., *ET AL.*: 'Mn-doped ZnO nanocrystals synthesized by sonochemical method: structural, photoluminescence, and magnetic properties', *Mater. Sci. Eng. B*, 2017, **219**, pp. 1–9

[24] Das S., Das S., Sutradhar S.: 'Enhanced dielectric behavior and ac electrical response in Gd–Mn–ZnO nanoparticles', *J. Alloys Compd.*, 2017, **726**, pp. 11–21

[25] Bououdina M., Omri K., El-Hilo M., *ET AL.*: 'Structural and magnetic properties of Mn-doped ZnO nanocrystals', *Physica E*, 2014, **56**, (2014), pp. 107–112

[26] Ogi T., Hidayat D., Iskandar F., *ET AL.*: 'Direct synthesis of highly crystalline transparent conducting oxide nanoparticles by low pressure spray pyrolysis', *Adv. Powder Technol.*, 2009, **20**, (2), pp. 203–209

[27] Du S., Tian Y., Liu H., *ET AL.*: 'Calcination effects on the properties of gallium-doped zinc oxide powders', *J. Am. Ceram. Soc.*, 2006, **89**, (8), pp. 2440–2443

[28] Chen X., He Y., Zhang Q., *ET AL.*: 'Fabrication of sandwich-structured ZnO/reduced graphite oxide composite and its photocatalytic properties', *J. Mater. Sci.*, 2010, **45**, (4), p. 953

[29] Zhang H., Yang D., Li S., *ET AL.*: 'Controllable growth of ZnO nanostructures by citric acid assisted hydrothermal process', *Mater. Lett.*, 2005, **59**, (13), pp. 1696–1700

[30] Moontragoon P., Pinitsoontorn S., Thongbai P.: 'Mn-doped ZnO nanoparticles: preparation, characterization, and calculation of electronic and magnetic properties', *Microelectron. Eng.*, 2013, **108**, pp. 158–162

[31] Zhao Y., Chen Y., Zhang X.C., *ET AL.*: 'Ultrafast all-optical switch using carbon nanotube polymer composites', US, 2002, A1[P], US 20020176650

[32] Deka S., Joy P.A.: 'Synthesis and magnetic properties of Mn doped ZnO nanowires', *Solid State Commun.*, 2007, **142**, (4), pp. 190–194

[33] Liao L., Liu Q.Y., Li C.: 'Effects of temperature on the ferromagnetism of Mn-doped ZnO nanoparticles and Mn-related Raman vibration', *Nanotechnology*, 2006, **17**, (5), p. 1520

[34] Wang M.H., Zhao Z.Y., Liu T.T.: 'Synthesis of Pr-doped ZnO nanoparticles by sol–gel method and varistor properties study', *J. Alloys Compd.*, 2015, **621**, pp. 220–224

[35] Sharma D., Jha R.: 'Analysis of structural, optical and magnetic properties of Fe/Co co-doped ZnO nanocrystals', *Ceram. Int.*, 2017, **43**, (11), pp. 8488–8496

[36] Nachaithong T., Thongbai P., Maensiri S.: 'Colossal permittivity in $(In_{1/2}\ Nb_{1/2})_xTi_{1-x}O_2$ ceramics prepared by a glycine nitrate process', *J. Eur. Ceram. Soc.*, 2017, **37**, pp. 655–660

[37] Wang M.H., Zhang B., Zhou F.: 'Preparation and characterization of CaCu 3 $Ti_4\ O_{12}$, powders by non-hydrolytic sol–gel method', *J. Sol-Gel Sci. Technol.*, 2014, **70**, (1), pp. 62–66